Monthly Notices
of the
ROYAL ASTRONOMICAL SOCIETY

MNRASL **436,** L99–L103 (2013) doi:10.1093/mnrasl/slt122
Advance Access publication 2013 September 25

Far-infrared spectroscopy of a lensed starburst: a blind redshift from *Herschel*

R. D. George,[1⋆] R. J. Ivison,[1,2] R. Hopwood,[3,4] D. A. Riechers,[5] R. S. Bussmann,[5] P. Cox,[6] S. Dye,[7] M. Krips,[6] M. Negrello,[8] R. Neri,[6] S. Serjeant,[4] I. Valtchanov,[9] M. Baes,[10] N. Bourne,[7] D. L. Clements,[3] G. De Zotti,[8,11] L. Dunne,[12] S. A. Eales,[13] E. Ibar,[14] S. Maddox,[12] M. W. L. Smith,[13] E. Valiante[13] and P. van der Werf[15]

[1]*Institute for Astronomy, University of Edinburgh, Blackford Hill, Edinburgh EH9 3HJ, UK*
[2]*UK Astronomy Technology Centre, Royal Observatory, Blackford Hill, Edinburgh EH9 3HJ, UK*
[3]*Physics Department, Imperial College London, South Kensington Campus, London SW7 2AZ, UK*
[4]*Department of Physical Sciences, The Open University, Milton Keynes MK7 6AA, UK*
[5]*Department of Astronomy, Space Science Building, Cornell University, Ithaca, NY 14853-6801, USA*
[6]*Institut de Radioastronomie Millimétrique, 300 rue de la Piscine, F-38406 Saint-Martin d'Hères, France*
[7]*School of Physics & Astronomy, University of Nottingham, University Park, Nottingham NG7 2RD, UK*
[8]*INAF, Osservatorio Astronomico di Padova, I-35122 Padova, Italy*
[9]*Herschel Science Centre, European Space Astronomy Centre, ESA, E-28691 Villanueva de la Cañada, Spain*
[10]*Sterrenkundig Observatorium, Universiteit Gent, Krijgslaan 281 S9, B-9000 Gent, Belgium*
[11]*SISSA, via Bonomea 265, I-34136 Trieste, Italy*
[12]*Department of Physics and Astronomy, University of Canterbury, Private Bag 4800, Christchurch, New Zealand*
[13]*School of Physics & Astronomy, Cardiff University, Queen's Buildings, The Parade 5, Cardiff CF24 3AA, UK*
[14]*Departamento de Astronomía y Astrofísica, Pontificia Universidad Católica de Chile, Vicuña Mackenna 4860, Casilla 306, Santiago 22, Chile*
[15]*Leiden Observatory, Leiden University, PO Box 9513, NL-2300 RA Leiden, the Netherlands*

Accepted 2013 August 19. Received 2013 August 15; in original form 2013 June 19

ABSTRACT

We report the redshift of HATLAS J132427.0+284452 (hereafter HATLAS J132427), a gravitationally lensed starburst galaxy, the first determined 'blind' by the *Herschel Space Observatory*. This is achieved via the detection of [C II] consistent with $z = 1.68$ in a far-infrared spectrum taken with the SPIRE Fourier Transform Spectrometer (FTS). We demonstrate that the [C II] redshift is secure via detections of CO $J = 2 \rightarrow 1$ and $3 \rightarrow 2$ using the Combined Array for Research in Millimeter-wave Astronomy and the Institut de Radioastronomie Millimétrique's Plateau de Bure Interferometer. The intrinsic properties appear typical of high-redshift starbursts despite the high lensing-amplified fluxes, proving the ability of the FTS to probe this population with the aid of lensing. The blind detection of [C II] demonstrates the potential of the SPICA Far-infrared Instrument imaging spectrometer, proposed for the much more sensitive Space Infrared Telescope for Cosmology and Astrophysics mission, to determine redshifts of multiple dusty galaxies simultaneously without the benefit of lensing.

Key words: galaxies: high-redshift – galaxies: starburst – infrared: galaxies – radio continuum: galaxies – radio lines: galaxies – submillimetre: galaxies.

1 INTRODUCTION

Through surveys using the Submillimetre Common-User Bolometer Array (Holland et al. 1999) came the discovery of a population of dust-obscured, submillimetre- (submm-)bright galaxies (Blain et al. 2002). Analogous to ultraluminous infrared galaxies in the local neighbourhood, these distant, gas-rich, intensely star-forming galaxies emit the bulk of their radiation in the rest-frame far-infrared (far-IR) waveband.

Surveys with the latest generation of far-IR- and submm-wavelength facilities, in particular the 3.5 m *Herschel Space Observatory*, have enabled us to image many more of these dusty star-forming galaxies (DSFGs) than was previously possible, over vastly larger areas, in up to five filters simultaneously, allowing us to probe rare populations that were not well-sampled in previous far-IR surveys.

The discovery of a bright, lensed population of DSFGs, intrinsically below the *Herschel* detection limit (e.g. Negrello et al. 2010), has confirmed that far-IR imaging is an efficient method by which to select strongly lensed objects and due to the sometimes high

⋆ E-mail: rdg@roe.ac.uk

magnification (e.g. $\mu = 37.5 \pm 4.5$; Swinbank et al. 2011), has permitted detailed studies of individual galaxies (e.g. Cox et al. 2011; Ivison et al. 2013).

High-resolution studies of individual DSFGs typically rely upon interferometric CO-line observations, necessitating precise knowledge of their redshifts. These remain notoriously difficult to obtain, due to the difficulty in pinpointing their positions and their faintness in the optical. However, the lensed DSFG population has proved to be within the reach of a range of new ground-based, broad-band spectroscopic instrumentation (e.g. Harris et al. 2012); very recently, Weiß et al. (2013) have demonstrated the power of ALMA, particularly at $z > 4$ where the 3 mm atmospheric window always contains a line.

Here, we present the first blind determination of a redshift using far-IR spectroscopic observations from space – a key step towards demonstrating the feasibility of integral-field far-IR spectroscopy as planned for the joint JAXA–ESA mission, Space Infrared Telescope for Cosmology and Astrophysics (SPICA; e.g. Swinyard et al. 2009). Throughout the Letter, we use *Wilkinson Microwave Anisotropy Probe* 7 cosmology (Komatsu et al. 2011) with $H_0 = 70.4\,\mathrm{km\,s^{-1}\,Mpc^{-1}}$, $\Omega_\mathrm{m} = 0.272$ and $\Omega_\Lambda = 0.728$.

2 DISCOVERY OBSERVATIONS

The North Galactic Pole is one of a number of fields observed as part of the *Herschel*–ATLAS (Eales et al. 2010) with *Herschel* (Pilbratt et al. 2010). The acquisition and reduction of parallel-mode data from SPIRE (Griffin et al. 2010) and PACS (Poglitsch et al. 2010) are described in detail by Ibar et al. (2010b), Pascale et al. (2011) and Rigby et al. (2011).

The SPIRE imaging led quickly to the selection of HATLAS J132427.0+284452 (hereafter HATLAS J132427) as a bright ($S_{350\,\mu\mathrm{m}} \gtrsim 200$ mJy; all bands $\geq 30\,\sigma$), potentially distant ($\{S_{250\,\mu\mathrm{m}}, S_{500\,\mu\mathrm{m}}\} < S_{350\,\mu\mathrm{m}}$), lensed starburst. This source is included in a number of follow-up campaigns, where we have been studying the brightest of these objects (e.g. Negrello et al. 2010; Fu et al. 2012; Omont et al. 2013).

The surface density of $S_{350\,\mu\mathrm{m}} \gtrsim 300$ mJy lens candidates is likely around 1/40 deg^{-2} (Negrello, private communication), plausibly placing this source among the most strongly lensed known DSFGs.

3 DETAILED FOLLOW-UP OBSERVATIONS

Much deeper PACS data were subsequently obtained from the OT1 programme, OT1_RIVISON_1, recording data simultaneously at 100 and 160 μm for a total of 6 min, and reaching $\sigma \approx 10$ and 12 mJy, respectively.

Approximately 30 min of high-resolution 7 GHz continuum data were acquired using the National Radio Astronomy Observatory's Jansky Very Large Array (NRAO's VLA) during 2011 June. The observation was performed in A configuration, with 64 × 2 MHz channels in each of two intermediate frequencies (IFs), each IF with dual polarization, recording data every 1 s. 3C 286 was observed every few minutes to determine accurate complex gain solutions and bandpass corrections and to set the absolute flux density scale. Using natural weighting, the resulting map has a circular 0.3 arcsec synthesized beam (full width at half-maximum, FWHM) and an rms. noise level of 10 μJy beam^{-1}.

870 μm imaging data were obtained using the Submillimeter Array (SMA) as part of programme 2011B-S044, with 9.7 h of total integration time in the compact, extended and very extended array configurations, with baselines covering 20–400 m, and the receivers tuned such that the upper sideband was centred on 870 μm.

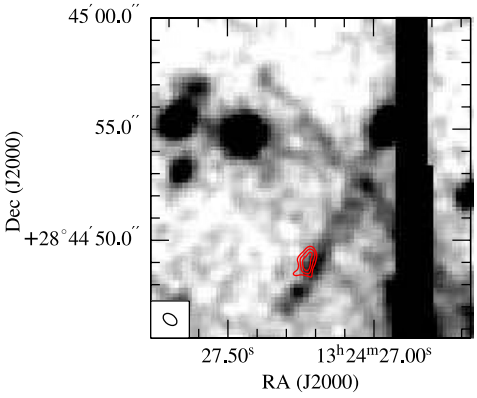

Figure 1. Continuum emission at 2 mm, as observed by PdBI with a 0.68 arcsec × 0.45 arcsec (PA 55°) synthesized beam, overlaid as contours on *r*-band imaging from the Canada–France–Hawaii Telescope (Gladders et al. 2003). The lensed arc is oriented NW–SE. The other elongated features are diffraction spikes caused by two bright, nearby stars. Both the brightest cluster galaxy and cluster centre are over 20 arcsec from the arc (Gladders & Yee 2005).

The blazar, 1924−292, was used as the bandpass calibrator and Titan was used for absolute flux calibration. The nearby quasar, 1310+323, was used to track the complex gains.

Following a tentative line detection using Zpectrometer on NRAO's Green Bank Telescope (GBT), plausibly CO $J = 1 \rightarrow 0$ at $z = 2.3078$ (Harris et al. 2012), we obtained 4.4 h on-source using all six of the 15 m antennas of the Institut de Radioastronomie Millimétrique's Plateau de Bure Interferometer (IRAM's PdBI). These data were taken during 2011 January, in A configuration, with the 2 mm receivers tuned to 139.380 GHz, corresponding to the rest-frame frequency of CO $J = 4 \rightarrow 3$ at that redshift. No CO line emission was visible within limits compatible with the $J = 1 \rightarrow 0$ flux and further follow-up of HATLAS J132427 was put on hold, pending a more robust redshift determination. We use these data here because they provide a usefully deep ($\sigma = 0.1$ mJy beam^{-1}), high-resolution [0.68 arcsec × 0.45 arcsec, position angle (PA) 55°] 2 mm continuum image.

Via our interferometric imaging shown in Fig. 1, it is immediately obvious that the far-IR source is coincident with the ∼10 arcsec giant arc reported by Gladders et al. (2003), strongly lensed by the rich foreground cluster RCS J132427+2845.2, at $z = 0.997 \pm 0.017$ (Gladders & Yee 2005).

4 FAR-IR AND CO SPECTROSCOPY

4.1 A blind redshift from the SPIRE FTS

During 2012 August 02, HATLAS J132427 was observed with a single pointing of the SPIRE Fourier Transform Spectrometer (FTS) for 3.8 h, the spectrum covering $\lambda_\mathrm{obs} = 194$–671 μm. The data were processed using the *Herschel* data processing pipeline (Fulton et al. 2010) within the HERSCHEL INTERACTIVE PROCESSING ENVIRONMENT v10. Spectra from detectors arranged around the central 'on-source' detector were averaged to produce a local background measurement, and subtracted from the source spectrum.

The $^2\mathrm{P}_{3/2} \rightarrow {}^2\mathrm{P}_{1/2}$ [C II] transition at rest-frame 157.74 μm is one of the brightest lines seen in the far-IR waveband, providing up to 1 per cent of L_IR (measured across rest-frame 8–1 000 μm) in star-forming galaxies (Stacey et al. 1991). Within the spectral range covered by the SPIRE FTS in our observations of lensed starburst

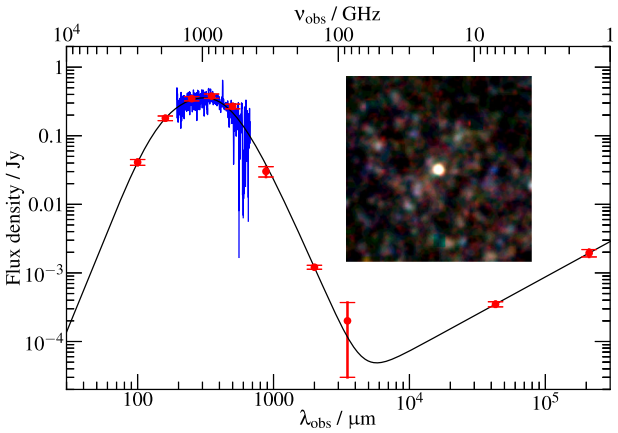

Figure 2. Far-IR-through-radio spectral energy distribution (SED) of HATLAS J132427, with the best-fitting synchrotron and power-law temperature distribution dust model shown in black. The FTS spectrum is shown in blue. Inset: 15 arcmin × 15 arcmin false-colour image of HATLAS J132427 in the three *Herschel* SPIRE filters.

Table 1. Continuum flux densities.

Wavelength	S_ν	Notes
100 μm	41 ± 4[a] mJy	*Herschel* PACS
160 μm	180 ± 14[a] mJy	*Herschel* PACS
250 μm	347 ± 25[b] mJy	*Herschel* SPIRE
350 μm	378 ± 28[b] mJy	*Herschel* SPIRE
500 μm	268 ± 21[b] mJy	*Herschel* SPIRE
870 μm	30.2 ± 5.2 mJy	SMA
2 mm	1.2 ± 0.1 mJy	IRAM's PdBI
3.5 mm	200 ± 170 μJy	CARMA
4.3 cm	350 ± 30 μJy	VLA
21 cm	1.95 ± 0.24 mJy	VLA (FIRST)

[a]Errors include 3 and 5 per cent calibration uncertainties at 100 and 160 μm, respectively.
[b]Errors include the contribution due to confusion and a 7 per cent calibration uncertainty has been added in quadrature (Valiante et al., in preparation).

galaxies, this line is likely to be the most significant; indeed, it is often the only transition detected (e.g. Ivison et al. 2010b).

The SPIRE FTS spectrum of HATLAS J132427, shown in Fig. 3, displays a 7.5 σ marginally resolved (1.2 GHz spectral resolution) emission line at (709.9 ± 0.4) GHz. Attributing this to [C II] indicates a redshift, $z = 1.677 \pm 0.001$. No other lines were detected, with $3\sigma < 200$, 230, 150, 600 Jy km s^{-1} for [O III] 88 μm, [N II] 122 μm, [O I] 145 μm and [N II] 205 μm, respectively, meaning that this redshift remained tentative at this point.

4.2 Redshift confirmation via CO

To verify the SPIRE FTS redshift determination, we used the Combined Array for Research in Millimeter-wave Astronomy (CARMA) to search for the CO $J = 2 \rightarrow 1$ line ($\nu_{rest} =$ 230.538 GHz), which should be redshifted to approximately $\nu_{obs} =$ 86.0 GHz for $z = 1.68$. Observations were carried out using the 3 mm receivers during 2012 November 23 in D configuration (11–146 m baselines), with 2.3 h spent on source. The blazars, 1310+323 and 0927+390, were used for complex gain calibration and to derive the bandpass shape. Absolute flux densities should be accurate to within ∼15 per cent. We obtained an 8σ detection of line emission, close to the expected frequency – see Fig. 4 – thus

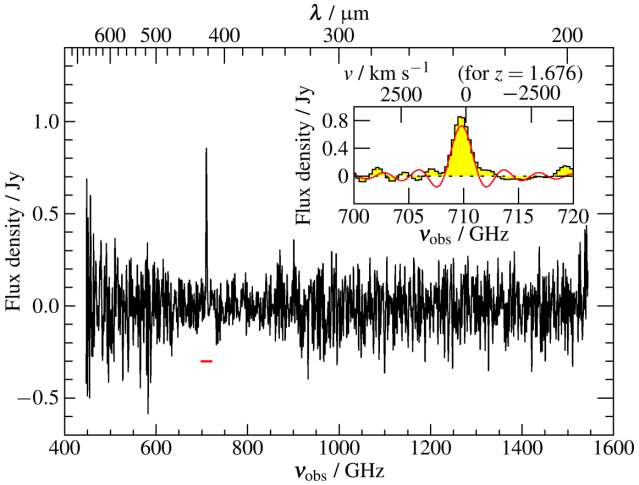

Figure 3. The continuum-subtracted *Herschel* SPIRE FTS spectrum. No other features correspond to expected transition lines. Inset: zoomed in on the region indicated by the red line in the parent plot. Velocity scale corresponds to [C II] at $z = 1.676$. The best-fitting sinc profile is overlaid in red.

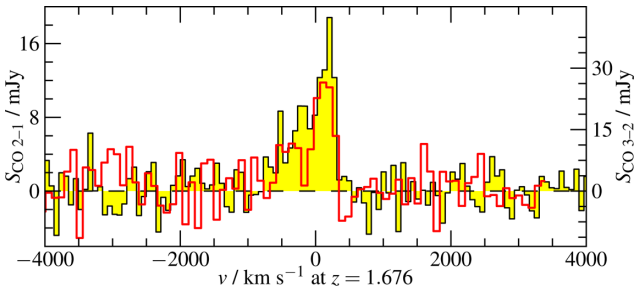

Figure 4. CO $J = 2 \rightarrow 1$ spectrum from CARMA, binned to 20.8 MHz, with the CO $J = 3 \rightarrow 2$ IRAM's PdBI spectrum shown in red, binned to 40 MHz and put on the same brightness temperature (T_b) scale.

confirming the redshift with $z = 1.676 \pm 0.001$. The 34.8 GHz GBT line is therefore presumably spurious.

We also imaged the source in CO $J = 3 \rightarrow 2$ with the IRAM's PdBI, also during 2012 November. We obtained 1.1 h of integration time, using all six of the 15 m antennas, this time in D configuration – the most compact. The observing frequency was set to 129.028 GHz, corresponding to the redshifted frequency of CO $J = 3 \rightarrow 2$ ($\nu_{rest} =$ 345.796 GHz) for $z = 1.68$. Again, we found a bright 3σ emission line at the expected frequency (Fig. 4).

The two line profiles are consistent with one another; neither can be described well with a single Gaussian, suggesting that their shape is due to either a merger or a rotating, gas-rich disc (e.g. Engel et al. 2010; Ivison et al. 2013). The line width (deduced from fits using a single Gaussian), 500 ± 140 km s^{-1} FWHM, is typical of those seen for DSFGs (Greve et al. 2005).

5 DISCUSSION

Characterization of the dust emission of HATLAS J132427 was performed by fitting the power-law dust temperature model of Kovács et al. (2010) to the continuum flux densities detailed in Table 1. This is shown in Fig. 2, with derived quantities detailed in Table 2.

Of the 350 ± 30 μJy integrated flux density at 7 GHz, 270 ± 25 μJy (77 ± 10 per cent) is in a compact component at RA = $13^h24^m27\overset{s}{.}225$, Dec. = $+28^\circ44'49\overset{''}{.}01$ (±0.02, J2000), with a best-fitting deconvolved size of 0.45 ± 0.05 arcsec × 0.09 ± 0.05 arcsec,

Table 2. Properties of HATLAS J132427.

Property	Value
T_d /K	33.1 ± 3.2
M_d / $10^9\,\mu^{-1}\,M_\odot$	1.07 ± 0.15
$A_{projected}{}^a$ /kpc^2	21.4 ± 5.7
L_{IR} /$10^{13}\,\mu^{-1}\,L_\odot$	2.91 ± 0.12
Synchrotron spectral index α	1.08 ± 0.09
q_{IR}	1.85 ± 0.09
SFR^b /$\mu^{-1}\,M_\odot\,yr^{-1}$	4 300
[C II] $I_{[CII]}$ /Jy km s^{-1}	486 ± 52
[C II] FWHM /km s^{-1}	800 ± 64
[C II] $L_{[CII]}$ /$10^{10}\,\mu^{-1}\,L_\odot$	5.80 ± 0.62
CO $J = 2 \rightarrow 1$ I_{CO} /Jy km s^{-1}	11.3 ± 1.4
CO $J = 2 \rightarrow 1$ FWHM /km s^{-1}	640 ± 270
CO $J = 2 \rightarrow 1$ L_{CO} /$10^8\,\mu^{-1}\,L_\odot$	1.64 ± 0.20
CO $J = 3 \rightarrow 2$ I_{CO} /Jy km s^{-1}	11.5 ± 3.5
CO $J = 3 \rightarrow 2$ FWHM^c /km s^{-1}	450 ± 170
CO $J = 3 \rightarrow 2$ L_{CO} /$10^8\,\mu^{-1}\,L_\odot$	2.50 ± 0.76
$r_{3-2/2-1}$	0.45 ± 0.15
$M_{gas}{}^d$ /$10^{11}\,\mu^{-1}\,M_\odot$	3.6 ± 0.6
SFE^d /$L_\odot\,M_\odot^{-1}$	83

[a]From fitting SED to dust emission.
[b]Following Murphy et al. (2011).
[c]From fitting a Gaussian with its mean constrained to that of the $J = 2 \rightarrow 1$ fit.
[d]Average determined via CO $J = 2 \rightarrow 1$ and $J = 3 \rightarrow 2$.

PA 152° ± 4°. Comparing this with the 2 mm emission (RA = 13^{h}24^{m}27^s.229 ± 0.004, Dec. = +28°44′49″.07 ± 0.06, J2000, 1.0 ± 0.2 arcsec × <0.3 arcsec, PA 152° ± 9°) suggests that the radio emission is significantly more compact than the dusty star-forming material, suggestive of a non-starburst origin. The radio spectral index, α (where $S_\nu \propto \nu^\alpha$) is steeper than the typical $\alpha = -0.8$, adding credibility to the idea that an AGN dominates the radio emission (e.g. Ibar et al. 2010a). Adopting the widely used parametrization of the far-IR/radio correlation, q_{IR} (with L_{IR} measured across rest-frame 8–1 000 μm), we find a value (1.85 ± 0.09) rather lower than that usually seen for DSFGs, ≈2.4 (Yun, Reddy & Condon 2001; Ivison et al. 2010a,b), again consistent with an AGN-related contribution to the radio luminosity (e.g. Donley et al. 2005).

The [O III] 88 μm line was not detected. An [O III] line of similar SNR to [C II] was observable from SDP.81 (which also has $q_{IR} \sim 1.8 \pm 0.1$ – Valtchanov et al. 2011), this time suggesting that the AGN has a greater influence in SDP.81 than in HATLAS J132427 (Abel et al. 2009).

CO is commonly used to trace molecular gas reservoirs. Estimates of the $J = 1 \rightarrow 0$ line flux can be derived from the higher-J line fluxes assuming Rayleigh–Jeans brightness temperature (T_b) ratios, e.g. $r_{2-1/1-0} \sim 0.84 \pm 0.13$ and $r_{3-2/1-0} \sim 0.52 \pm 0.09$ (Ivison et al. 2011; Bothwell et al. 2013): consistent with the T_b ratio measured here for $r_{3-2/2-1}$, 0.45 ± 0.15. Adopting $\alpha_{CO} = 0.8\,M_\odot\left(K\,km\,s^{-1}pc^2\right)^{-1}$, as is usual for starburst galaxies (e.g. Bolatto, Wolfire & Leroy 2013), we derive a H_2 + He mass, $M_{gas} = (3.6 \pm 0.6) \times 10^{11}\,\mu^{-1}\,M_\odot$, having averaged the $J = 2 \rightarrow 1$ and $3 \rightarrow 2$ measurements. Following Harris et al. (2012) and Bothwell et al. (2013), a rough magnification estimate can be derived from the $J = 1 \rightarrow 0$ luminosity and linewidth, yielding $\mu \approx 11$.

An independent estimate of the gas mass can be derived via the gas-to-dust mass ratio, M_{gas}/M_d. For 1/3 Solar metallicity, this is 220^{+180}_{-90} (Sandstrom et al. 2012), suggesting $M_{gas} = 2.4^{+2.0}_{-1.0} \times 10^{11}\,\mu^{-1}\,M_\odot$, consistent with our CO-based estimate, albeit with a large uncertainty. These estimates of the gas mass correspond to a star formation efficiency $60 \lesssim L_{IR}/M_{gas} \lesssim 220\,L_\odot\,M_\odot^{-1}$, and a gas-consumption time-scale $M_{gas}/SFR \sim 30-100$ Myr, consistent with those typically measured for DSFGs (e.g. Greve et al. 2005).

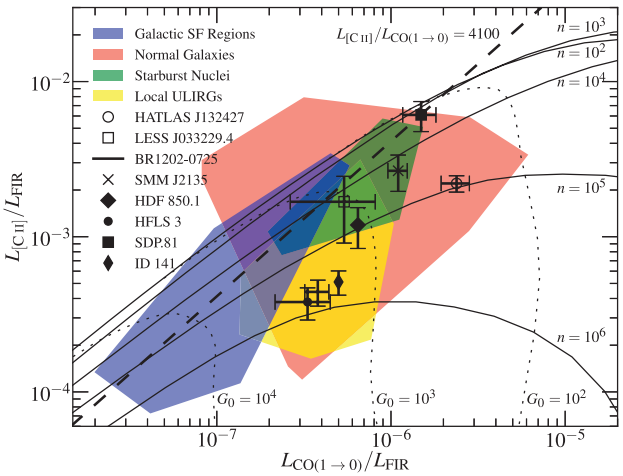

Figure 5. Diagnostic plot, adapted from Hailey-Dunsheath et al. (2010), with identical corrections applied to $L_{[C\,II]}$ (× 0.7 – non-PDR emission) and L_{CO1-0} (×2.0 – an optically thick transition). Shaded regions are approximate coverage of local objects. Neglecting differential lensing magnification, n and G_0 estimates are magnification-independent. Also, shown are other high-redshift starbursts: LESS J033229.4−275619 (De Breuck et al. 2011), BR 1202−0725 (Wagg et al. 2012), SMM J2135−0102 (Ivison et al. 2010b), HDF 850.1 (Walter et al. 2012), HFLS 3 (Riechers et al. 2013), *H*-ATLAS SDP.81 (Valtchanov et al. 2011) and HATLAS ID 141 (Cox et al. 2011). Where necessary, literature values have been converted using $r_{2-1/1-0} \sim 0.84 \pm 0.13$, and the ratios obtained by integrating under the HATLAS J132427 SED: $L_{FIR(42.5-122.5\,\mu m)} = 0.69 \times L_{(40-500\,\mu m)} = 0.63 \times L_{IR(8-1000\,\mu m)}$.

Using the photodissociation region (PDR) model displayed in Fig. 5, representing the far-UV-illuminated surface of an interstellar cloud, we estimate $n \sim 10^{4.8}$ cm^{-3} and $G_0 \sim 10^{2.3}$, a density and far-UV radiation field strength comparable with other high-redshift starbursts. These models assume that all CO emission is produced in PDRs, neglecting any contribution from quiescent gas or turbulent heating which provide plausible explanations for the comparatively large $L_{CO(1\rightarrow0)}/L_{FIR}$ in this object, as may increased metallicity. Differential magnification might also affect these derived properties, if the CO and far-IR emission are not co-spatial (e.g. Fu et al. 2012).

Without a detailed mass model of the cluster lens, it is not possible to investigate the extent of differential magnification of the DSFG, but we can nonetheless attempt a plausibility test of the statistical likelihood. Following Serjeant (2012), we modelled a singular isothermal ellipsoid with a 20 arcsec critical radius and ellipticity of 0.2, with the same submm galaxy model used in that paper. As with the galaxy-scale lenses in Serjeant (2012), we found Fig. 5 to be largely unaffected by differential magnification, even for $\mu > 10$. However, the aspect ratio of the observed-frame optical emission suggests a high magnification and large angular extent, implying long-baseline interferometric measurements may resolve out some of the emission, as discussed in Section 4.2.

6 IMPLICATIONS FOR FAR-IR INTEGRAL-FIELD SPECTROSCOPY

SPICA (Swinyard et al. 2009) is a planned successor to *Herschel*. Thermal emission from the 80 K primary telescope of *Herschel* is six orders of magnitude brighter than the far-IR background; with a

dish temperature of 6 K, SPICA should be two orders of magnitude more sensitive than any previous far-IR facility.

The SPICA FAR-infrared Instrument (SAFARI) is an imaging FTS proposed for SPICA, covering 34–210 μm ([O I] 63 μm to $z = 2.3$) over a 2 arcmin × 2 arcmin field of view with an intended spectral resolution $R \sim 2000$ and sensitivity $<$ few $\times 10^{-19}$ W m^{-2} (5σ : 1 h; Swinyard et al. 2009).

Our observation of [C II] from HATLAS J132427 provides $I_{[\mathrm{C\,II}]} = (1.15 \pm 0.12) \times 10^{-17}$ W m^{-2}. An [O I] line of this flux will likely be observable to several σ within 2 s of integration with SPICA. While such sources will likely be known before a SPICA pointing, the ability of *Herschel* to obtain a blind redshift provides confidence that with observations of order 1 h, the much more sensitive SPICA will pinpoint redshifts of multiple unlensed few mJy cosmic infrared background (CIB) sources (potentially several from each spectrum – Clements et al. 2007; Raymond et al. 2010), reducing the need for the blind CO line searches typically required today. With such integration times, blind fine-structure line detections are feasible and a gateway to detailed imaging/dynamical studies with ALMA.

7 CONCLUSIONS

We present the first blind redshift to have been obtained via *Herschel* spectroscopy. The galaxy, at $z = 1.68$, is lensed by a rich galaxy cluster at $z = 1.0$ into an arc of length ∼10 arcsec. A lensing model will be presented in Fu et al. (in preparation).

This source appears to be a disc-like system, with a best-fitting L_{IR} of $2.91 \times 10^{13}\,\mu^{-1}\,\mathrm{L}_{\odot}$, dust temperature of $T_{\mathrm{d}} = 33$ K and SFR of $4300\,\mu^{-1}\,\mathrm{M}_{\odot}\,\mathrm{yr}^{-1}$, and a compact AGN-related contribution to the radio flux density.

The observed [C II] flux is $(1.15 \pm 0.12) \times 10^{-17}$ W m^{-2}, suggesting an [O I] line of similar flux could be detected by SPICA to 5σ with an integration time of order 3 s. Even many unlensed DSFGs may require no more than ≈1 h of integration. The feasibility of blind line detections will not only directly advance our knowledge of high-redshift systems and their interstellar media, but act as a gateway to detailed imaging and spectral studies with (sub-)millimetre interferometers such as ALMA.

ACKNOWLEDGEMENTS

We thank Howard Yee and Michael Gladders for providing the CFHT image. RDG acknowledges support from STFC. RJI acknowledges support from the European Research Council (ERC) in the form of Advanced Grant, COSMICISM. The *Herschel*-ATLAS is a project with *Herschel*, which is an ESA space observatory with science instruments provided by European-led Principal Investigator consortia and with important participation from NASA. The *H*-ATLAS website is http://www.h-atlas.org/. US participants in *H*-ATLAS acknowledge support from NASA through a contract from JPL. IRAM is supported by INSU/CNRS (France), MPG (Germany) and IGN (Spain). Support for CARMA construction was derived from the states of California, Illinois and Maryland, the James S. McDonnell Foundation, the Gordon and Betty Moore Foundation, the Kenneth T. and Eileen L. Norris Foundation, the University of Chicago, the Associates of the California Institute of Technology and the National Science Foundation (NSF). Ongoing CARMA development and operations are supported by the NSF under a cooperative agreement and by the CARMA partner universities. The NRAO is a facility of the NSF operated under cooperative agreement by Associated Universities, Inc. The SMA is a joint project between the Smithsonian Astrophysical Observatory and the Academia Sinica Institute of Astronomy and Astrophysics and is funded by the Smithsonian Institution and the Academia Sinica.

REFERENCES

Abel N. P., Dudley C., Fischer J., Satyapal S., van Hoof P. A. M., 2009, ApJ, 701, 1147
Blain A. W., Smail I., Ivison R. J., Kneib J.-P., Frayer D. T., 2002, Phys. Rep., 369, 111
Bolatto A. D., Wolfire M., Leroy A. K., 2013, ARA&A, 51, 207
Bothwell M. S. et al., 2013, MNRAS, 429, 3047
Clements D. L., Isaak K. G., Madden S. C., Pearson C., 2007, A&A, 465, 125
Cox P. et al., 2011, ApJ, 740, 63
De Breuck C., Maiolino R., Caselli P., Coppin K., Hailey-Dunsheath S., Nagao T., 2011, A&A, 530, L8
Donley J. L., Rieke G. H., Rigby J. R., Pérez-González P. G., 2005, ApJ, 634, 169
Eales S. et al., 2010, PASP, 122, 499
Engel H. et al., 2010, ApJ, 724, 233
Fu H. et al., 2012, ApJ, 753, 134
Fulton T. R. et al., 2010, in Oschmann J. M., Jr, Clampin M. C., MacEwen H. A., eds, Proc. SPIE Conf. Ser. Vol. 7731, Space Telescopes and Instrumentation 2010: Optical, Infrared, and Millimeter Wave. SPIE, Bellingham, p. 773134
Gladders M. D., Hoekstra H., Yee H. K. C., Hall P. B., Barrientos L. F., 2003, ApJ, 593, 48
Gladders M. D., Yee H. K. C., 2005, ApJS, 157, 1
Greve T. R. et al., 2005, MNRAS, 359, 1165
Griffin M. J. et al., 2010, A&A, 518, L3
Hailey-Dunsheath S., Nikola T., Stacey G. J., Oberst T. E., Parshley S. C., Benford D. J., Staguhn J. G., Tucker C. E., 2010, ApJ, 714, L162
Harris A. I. et al., 2012, ApJ, 752, 152
Holland W. S. et al., 1999, MNRAS, 303, 659
Ibar E., Ivison R. J., Best P. N., Coppin K., Pope A., Smail I., Dunlop J. S., 2010a, MNRAS, 401, L53
Ibar E. et al., 2010b, MNRAS, 409, 38
Ivison R. J. et al., 2010a, A&A, 518, L31
Ivison R. J. et al., 2010b, A&A, 518, L35
Ivison R. J., Papadopoulos P. P., Smail I., Greve T. R., Thomson A. P., Xilouris E. M., Chapman S. C., 2011, MNRAS, 412, 1913
Ivison R. J. et al., 2013, ApJ, 772, 137
Komatsu E. et al., 2011, ApJS, 192, 18
Kovács A. et al., 2010, ApJ, 717, 29
Murphy E. J. et al., 2011, ApJ, 737, 67
Negrello M. et al., 2010, Sci, 330, 800
Omont A. et al., 2013, A&A, 551, A115
Pascale E. et al., 2011, MNRAS, 415, 911
Pilbratt G. L. et al., 2010, A&A, 518, L1
Poglitsch A. et al., 2010, A&A, 518, L2
Raymond G., Isaak K. G., Clements D., Rykala A., Pearson C., 2010, PASJ, 62, 697
Riechers D. A. et al., 2013, Nat, 496, 329
Rigby E. E. et al., 2011, MNRAS, 415, 2336
Sandstrom K. M. et al., 2012, preprint (arXiv:1212.1208)
Serjeant S., 2012, MNRAS, 424, 2429
Stacey G. J., Geis N., Genzel R., Lugten J. B., Poglitsch A., Sternberg A., Townes C. H., 1991, ApJ, 373, 423
Swinbank A. M. et al., 2011, ApJ, 742, 11
Swinyard B. et al., 2009, Exp. Astron., 23, 193
Valtchanov I. et al., 2011, MNRAS, 415, 3473
Wagg J. et al., 2012, ApJ, 752, L30
Walter F. et al., 2012, Nat, 486, 233
Weiß A. et al., 2013, ApJ, 767, 88
Yun M. S., Reddy N. A., Condon J. J., 2001, ApJ, 554, 803

This paper has been typeset from a TEX/LATEX file prepared by the author.